Journal of Engineering Science 15(2), 2024, 29-39
DOI: https://doi.org/10.3329/jes.v15i2.82160

JES
an international Journal

HIGHLY EFFECTIVE REMOVAL OF CIPROFLOXACIN FROM AQUEOUS SOLUTION USING GRAPHENE OXIDE FUNCTIONALIZED ZEOLITE

Md. S. Ahmmed[1] and A. K. Mohiuddin[1]*

[1] Department of Chemistry, University of Dhaka, Dhaka-1000, Bangladesh

Received: 22 August 2024 Accepted: 02 December 2024

ABSTRACT

Graphene oxide (GO) functionalized zeolites (ZGO) was synthesized as an adsorbent for swift and successful removal of the ciprofloxacin (CIP) antibiotic. The as-prepared nanocomposite was characterized by field emission scanning electron microscopy (FESEM), Fourier transform infrared spectroscopy (FTIR), and RAMAN spectroscopy. The adsorption ability of ZGO for CIP was investigated at different pH (2-11), contact time (5-120 min), and adsorbent dosage (0.1-0.75 g L^{-1}) to obtain the optimum condition for maximum removal percentage of target adsorbate. The results provided very fast (15 min only) highly effective removal of CIP (97.67%) for 0.25 g L^{-1} ZGO, while the pH of the aqueous solution was 7.0. Kinetic and isotherm analysis of this study indicated that the adsorption process happened on the multilayer and heterogeneous surface of ZGO and was carried out by a chemical reaction between CIP and ZGO. The highest adsorption capacity (q_m) was calculated as 61.35 mg g^{-1} at 40°C, while 8.28 and 12.45 mg g^{-1} were at 20, and 30°C, respectively, which suggested the stimulation of greater sites of ZGO surface with the increment of temperatures during the adsorption process. Furthermore, strong stability and superior reusability of ZGO revealed that it could be a potential adsorbent for easy removal of CIP antibiotics from the aqueous solution.

Keywords: *Functionalized GO, Ciprofloxacin antibiotic, Adsorbent, Adsorbate, Zeolites*

1. INTRODUCTION

Currently, safe water availability is a great challenge due to its necessity for all existing creatures of the universe. Regular surveillance of ground and surface water is very essential since all living animals, plants, and human beings are directly dependent on them (Mohiuddin *et al*., 2021; Samal *et al*., 2022). We should take appropriate steps to secure germ-free, immaculate surface water for significant human health and environmental sustainability (Igwegbe *et al*., 2021). However, the surface water is sometimes polluted by various chemicals, especially widely used antibiotics, pesticides, and heavy metals (Walker *et al*., 2019). Pharmaceutical contaminants (PCs) are a unique group of emerging contaminants of global concern due to their persistent nature in the natural ecosystem, genotoxic and mutagenic effects on human and aquatic lives, and difficulties in degradation through conventional techniques (Akpotu *et al*., 2019; Magesh *et al*., 2022).

Recently, the manufacturing and consumption of antibiotics have expanded significantly due to their wide uses in agriculture, animal husbandry, and pathogens' resistance to antibiotics (Al-Musawi *et al*., 2021; Tang *et al*., 2017). Ciprofloxacin (CIP) is a synthetic antibiotic and broadly used to treat chest, skin, and bone bacterial infections (Zhu *et al*., 2015; Pham *et al*., 2020). CIP is extremely soluble in water (≈1.35 mg mL^{-1}) (Kümmerer *et al*., 2009), and it is arduous to degrade in nature due to the presence of fluorine atoms (Mohammed *et al*., 2019). Recently, the existence of CIP residue has been reported in the range of 100 ng L^{-1} to 10 µg L^{-1} in the wastewater, one hundred ng L^{-1} to µg L^{-1} in surface water, 25 µg L^{-1} in the environment, and from 100 to 500 mg L^{-1} in industrial and hospital effluents (Jara-Cobos *et al*., 2023; Ghosh *et al*., 2023; Antonelli *et al*., 2020; Tran *et al*., 2022). These remarkable CIP concentrations in the wastewater and soil could cause antibiotic-resistance bacteria as well as be responsible for serious health threats such as salmonella typhimurium, which leads to genotoxic effects on aquatic organisms (Diwan *et al*., 2010; Espinosa *et al*., 2015; Cox *et al*., 2002; Kummerer *et al*., 2000; Bui *et al*., 2013; Van Wieren *et al*., 2012). It is highly necessary to remove CIP from wastewater due to the concern for human health, the environment, and the ecosystem. There are numerous techniques such as photocatalytic degradation (Dao *et al*., 2018), advanced oxidation (Karthikeyan *et al*., 2012; Biancullo *et al*., 2019), membrane process (Radjenović *et al*., 2008; Tran *et al*., 2016; Tran *et al*., 2017), ozonation (Moreira *et al*., 2016), bioremediation (Polesel *et al*., 2016; Sarangapani *et al*., 2019), and adsorption (Grimes *et al*., 2019; Le *et al*., 2018; Tran *et al*., 2019) for antibiotic removal that have been introduced. Out of them, the adsorption process offers superior advantages because of its simple procedure, easy maintenance, low cost, and low eco-friendliness (Ahmed *et al*., 2015; Homem *et al*., 2011).

*Corresponding Author: *akmohiuddin.che@du.ac.bd*

ISSN 2075-4914 (print); ISSN 2706-6835 (online)

Zeolites are microporous aluminosilicate crystalline minerals with 3-dimensional frameworks of SiO_4 and AlO_4 tetrahedra that are linked through oxygen atoms to give orderly interconnected cages and tunnels (Chen *et al*., 2015; Yu *et al*., 2013). Recently, zeolites have been used frequently in the adsorption process due to their microporosity, large surface area, low cost, thermal stability, and high cation-exchange capacity (Cheng *et al*., 2017). But the smaller pore size of zeolites compared to the molecular size of the antibiotics restrains their broad application for wastewater treatment (Farghali *et al*., 2021). Surface modification and/or functionalization could be a simple technique to overcome this problem as well as enhance the adsorption performances of zeolites (Mohiuddin *et al*., 2022). GO, one of the most remarkable inventions of the twentieth century, could modify the surface area and porosity of zeolites to improve their adsorption capacity towards adsorbents. The adsorption capacity of GO for CIP and Cs (I) from water was reported as 18.6 and 32.53 mg g^{-1}, respectively (Yadav *et al*., 2018; Tan *et al*., 2016). The adsorption capacities of reduced GO-modified magnetite composites and GO-modified zeolite for CIP and rhodamine B were determined as 18.2 and 55.56 mg g^{-1}, respectively (Tang *et al*., 2013). But GO is highly dispersible in water, and it is hard to distinguish the dispersed GO after completing the adsorption process from the wastewater (Farghali *et al*., 2021). In order to solve the separation problem of GO and overcome the pore size trouble of zeolites, GO functionalized zeolite was proposed for the effective removal of CIP from the aqueous solution.

In this study, GO functionalized zeolite (ZGO) was synthesized through a simple hydrothermal process. The successful formation of ZGO was confirmed by FESEM, FTIR, and RAMAN. The adsorption ability of ZGO for CIP was examined by different parameters such as pH of the aqueous solution, contact time of the adsorption process, dosages of ZGO, initial CIP concentration, and temperature. Kinetic and isotherm analysis were obtained as a function of the variable of contact time and the initial concentration of CIP, respectively. For adsorption kinetics, the experimental data were fitted to pseudo-first-order, pseudo-second-order, Elovich, and intra-particle diffusion models, whereas analyzed Langmuir, Freundlich, and Temkin models for adsorption isotherms**.**

2. EXPERIMENTAL

2.1 Synthesis of Zgo

Following a modified version of the Hummer's method, GO was obtained from graphite powder (Mohiuddin *et al*., 2021). Firstly, 2.0 g zeolite was added to the mixture of 1.0 mL concentrated H_2SO_4 and 25.0 mL distilled water (DW) in a 100 mL round-bottomed flask. After sonication for 30 min, 1 mg mL^{-1} GO dispersion dropwise was added into the flask. After completing the reaction, the reaction composition was refluxed for 24 h under magnetic stirring at 100 °C. After that, the mixture was kept overnight to settle down. Then, the homogeneous mixture was centrifuged at 4000 rpm and washed with DW and absolute ethanol (EtOH). The obtained black powder was finally dried (50°C, 12 h) in a vacuum oven, and 1.9139 g of ZGO was collected.

2.2 Adsorption Studies

100 mg L^{-1} stock aqueous solution of CIP was prepared in methanol from standard 1000 mg L^{-1} CIP adsorbate and reserved in the refrigerator. The pH of the aqueous solution was prepared and controlled by using 0.1 M H_3PO_4 and 0.1 M NaOH. For adsorption studies, the initial concentration of CIP solution was 0.4 mg mL^{-1}. Following that, a certain amount of ZGO was put in the CIP solution and shaken at 200 rpm at room temperature (RT) using an orbital shaker. After a definite shaking time, the solution of ZGO and CIP was centrifuged at 4000 rpm and separated the residue with a 0.45 µm CHROMAFIL® Xtra syringe filter. The blank concentration (without adsorption) and different concentrations of adsorption of CIP by different dosages of ZGO were measured by a LC-MS/MS (Agilent 1290 TQ 6420) in positive electron spray ionization mode (ESI+). The adsorption ability of ZGO for CIP was determined by Equation (1).

$$\text{Removal percentage} = \frac{C_o - C_t}{C_o} \times 100 \quad (1)$$

where C_o is the initial, and C_t is the concentration at time t (mg L^{-1}) of CIP solution. Adsorbed amount of CIP by ZGO at time t (q_t), and at equilibrium (q_e) were determined by Equations (2) and (3), respectively.

$$q_t = \frac{C_o - C_t}{M} \times V \quad (2)$$

$$q_e = \frac{C_o - C_e}{M} \times V \quad (3)$$

where *Ce* is the equilibrium concentration of CIP solution (mg L^{-1}). *M* and *V* represent the dosage of ZGO (g), and the volume (L) of CIP solution.

3. RESULTS AND DISCUSSION

3.1 Characterization

3.1.1 *Morphology Analysis*

FESEM was conducted to study the surface morphologies of GO and ZGO. Figure 1a exhibited a well-packed layered structure of GO with wave-like cloud morphology (Gurunathan *et al*., 2016). Figures 1b to 1d revealed the FESEM images of ZGO at different magnifications. Figure 1b showed the scatter distribution of numerous numbers of zeolites nanoparticles (NPs) on the GO surface, whereas Figure 1c illustrated that the GO surface was decorated with different diameters of zeolites nanoparticles. Figure 1d demonstrated that the crystal shape of zeolite nanoparticles was cubic (Li *et al*., 2020).

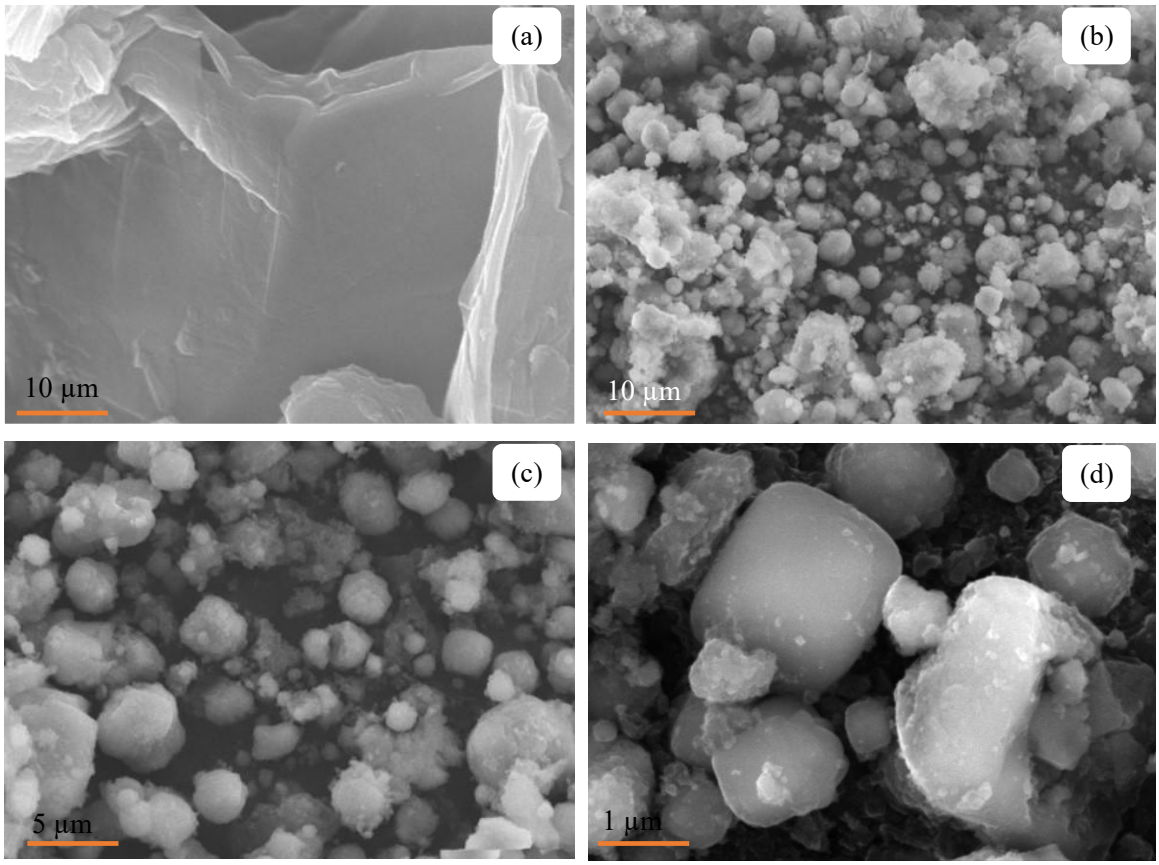

Figure 1: FESEM images of (a) GO, and (b-d) ZGO at different magnifications.

3.1.2 *Structural Analysis*

FTIR was investigated to analyze the bonding configuration of GO and ZGO. Figure 2a exhibited the FTIR spectra of GO and ZGO. GO showed characteristic peaks at 1052 cm^{-1}, 1234 cm^{-1}, 1629 cm^{-1}, and 1733 cm^{-1}, which were due to stretching vibration of alkoxy C-O, stretching vibration of epoxy C-O, stretching vibration of C=C, and stretching vibration of C=O, respectively. Furthermore, a weak peak at 1409 cm^{-1} and a wide peak at 3324 cm^{-1} were due to O-H deformation and stretching and vibration of O-H, respectively (Mohiuddin *et al*., 2023). On the other hand, ZGO showed characteristic peaks at 460 cm^{-1}, 594 cm^{-1}, and 1004 cm^{-1}, which were due to internal vibrations of MO_4 (M = Al/Si). Moreover, the disappearance of stretching vibration of C=O peaks (1733 cm^{-1}) and shifting of the stretching and vibration O-H peaks to ~3356 cm^{-1} indicated that the -C=O- groups might have been converted to Al/Si-O-C bonds, resulting in the formation of the ZGO nanocomposite (Choudhury *et al*., 2021; Huang *et al*., 2012).

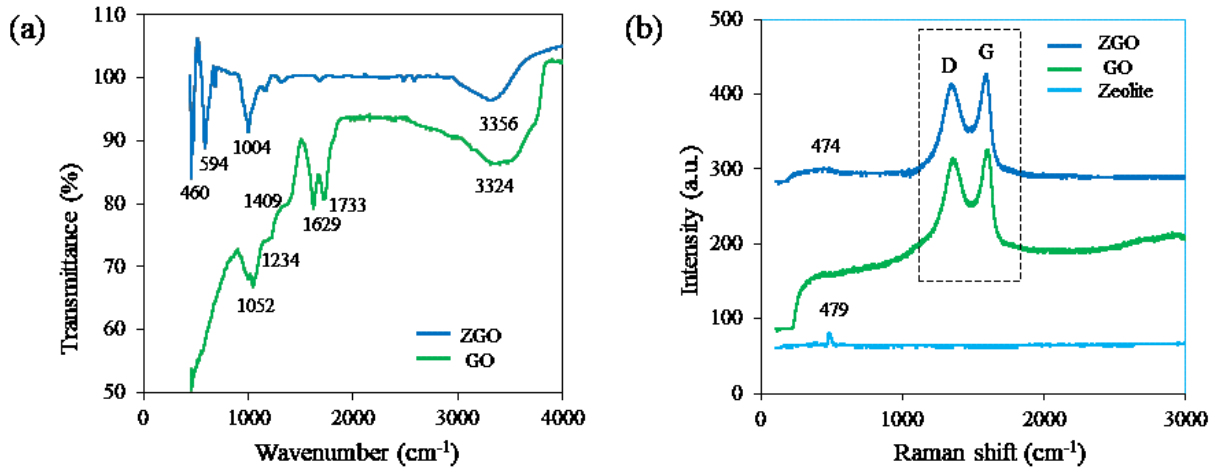

Figure 2: (a) FTIR spectra of GO, and ZGO, and (b) Raman spectra of GO, and ZGO with zeolite as reference.

Raman spectroscopy was examined to study the chemical structure and molecular interactions of the prepared samples. Figure 2b exhibited the Raman spectra of zeolites, GO, and ZGO. A sharp peak at ~479 cm^{-1} in the zeolites sample corresponds to M-O in the zeolite structure (Yu *et al*., 2013). The D and G bands of GO materialized at ~1353 cm^{-1} and ~1596 cm^{-1}, respectively, which slightly shifted to ~1348 cm^{-1} (5 cm^{-1}) and ~1594 cm^{-1} (2 cm^{-1}) for ZGO. This red shift indicated the remarkable bond configuration between the M-O bond of zeolites and the carbon atom of the GO plane (Banu *et al*., 2020). Furthermore, ZGO also showed a slight change in peak position (at ~474 cm^{-1}), which suggested the existence of zeolites on the GO surface.

3.2 Optimization of the Experimental Conditions

3.2.1 *pH Effect*

The pH significantly controls the removal percentage of CIP in the aqueous solution. Figure 3a showed the influence of different pH (2-11) in the removal percentages of CIP for the 0.25 g L^{-1} ZGO at 15 min. The figure demonstrated that the removal percentages of CIP improved step by step from pH 2.0 to 7.0, then declined from pH 7.0 to 11.0. CIP is mostly anionic (CIP^-, deprotonated due to COOH) at pH > 8.7, zwitterionic (neutral CIP) in the range of pH 6.1 to pH 8.7 and cationic (CIP^+, deprotonated due to NH2) at < 6.1 (Wang *et al*., 2016). On the other hand, the COOH group of ZGO has a pKa of 4.5 (Chen *et al*., 2015). At pH 2.0, the removal percentage of CIP was lowest due to all neutral COOH species of ZGO and the largest amount of CIP in the aqueous solution. With the increasing of pH, the COOH group of ZGO started to deprotonate and turned into negatively charged COO^-. At pH 4.5, around 85% of the CIP^+ is adsorbed by negatively charged ZGO. In the range of pH 4.5 to 6.1, electrostatic repulsion occurs due to positively charged ZGO and CIP^+. At pH 5.0, about 80% of the -COOH group deprotonated (COO^-), while at pH 9.0, all -COOH groups deprotonated (Chen *et al*., 2015). At pH 6.1, around 95% of the CIP adsorbed by ZGO and adsorption process still increased instead of positively charged ZGO and neutral CIP. It may be due to the H-bonding or electron acceptor mechanism between ZGO and CIP (Alameri *et al*., 2022). At pH 7.0, the maximum removal of CIP was 96.77%.

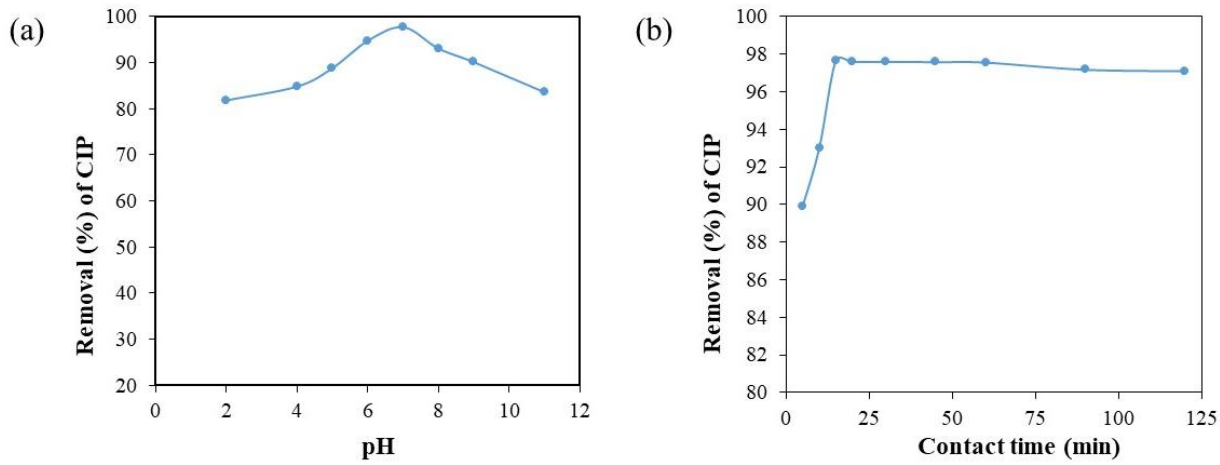

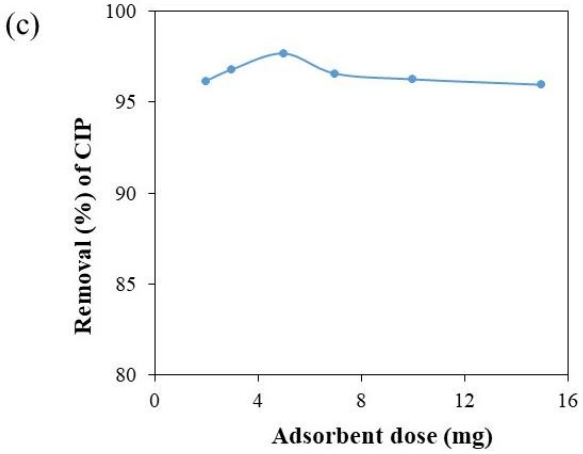

Figure 3: (a) Effect of pH on the adsorption of CIP from the aqueous solution by ZGO (Co = 100 mg L^{-1}, ZGO = 0.25 g L^{-1}, t = 15 min, shaking = 200 rpm, T = 32 °C), (b) effect of contact time on the adsorption of CIP by ZGO (Co = 100 mg L^{-1}, ZGO = 0.25 g L^{-1}, pH = 7, shaking = 200 rpm, T = 32 °C), and (c) effect of adsorbent dose on the adsorption of AZM from the aqueous solution onto ZGO (Co = 100 mg L^{-1}, pH = 7, t = 15 min, shaking = 200 rpm, T = 32 °C).

3.2.2 *Effect of Contact Time*

Contact time is the foremost consideration for economical and effective removal of selective pollutants in the wastewater treatment process. Figure 3b showed the influence of different contact times (5–120 min) in the removal percentages of CIP for the 0.25 g L^{-1} ZGO at pH 7.0. The figure illustrated that the removal percentages of CIP sharply increased from 1 to 15 min, then remained almost constant up to 120 min. Initially, the adsorption of CIP by ZGO was very low due to the lack of enough time for physical contact for the chemical reaction (Alameri *et al*., 2022). At 5 minutes, it was almost 90% due to the large amount of CIP and lot of free active sites of ZGO [54]. At 15 minutes, saturation occurs and the chemical reaction reaches equilibrium. The maximum removal of CIP was 97.67% at 15 min.

3.2.3 *Effect of Adsorbent Dosage*

Figure 3c showed the influence of different amounts of ZGO (2–15 mg) in the removal percentages of CIP for 15 min at pH 7.0. The figure exhibited that the removal percentages of CIP improved gradually from 96.15 to 97.67% for 2 to 5 mg of ZGO, which reflects the identical concurrence with previously reported zeolites adsorbent (Samarghandi *et al*., 2015). Then the removal percentages of CIP decreased and remained almost constant up to 15 mg due to aggregation of the adsorbent. 5 mg (0.25 g L^{-1}) was selected as the optimum dosage of ZGO for this study.

3.2.4 *Adsorption Kinetics*

To get information about the physical and/or chemical interaction between CIP and ZGO, the adsorption kinetics were investigated. The mathematical linear forms of pseudo-first-order (equation 4: where, k_1 is the pseudo-first-order rate constant, g mg^{-1} min^{-1}), pseudo-second-order (equation 5: where, k_2 is the pseudo-second-order rate constant, g mg^{-1} min^{-1}), Elovich (equation 6: where, a_e and b_e is the initial adsorption rate, mg g^{-1} min^{-1}; and magnitude of surface coverage and activation energy for chemisorption, g mg^{-1}, respectively), and intra-particle diffusion (equation 7: where, k_i and C_i is the rate constant associated with the intra-particle diffusion model, mg g^{-1} $min^{-0.5}$; and the constant and proportional to boundary layer thickness, mg g^{-1}, respectively), were calculated for 0.5 mg L^{-1} initial concentration of CIP and 0.25 g L^{-1} adsorbent dose of ZGO at pH 7.0 for 5-120 min at RT (Wahab *et al*., 2021; Azam *et al*., 2022; Upoma *et al*., 2022).

$$\ln(q_e - q_t) = \ln q_e - k_1 t \quad (4)$$

$$\frac{t}{q_t} = \frac{1}{k_2 q_e^2} + \frac{t}{q_e} \quad (5)$$

$$q_t = \frac{\ln a_e b_e}{b_e} + \frac{1}{b_e} \ln t \quad (6)$$

$$q_t = k_i t^{0.5} + C_i \quad (7)$$

Figure 4 shows the calibration curves for four kinetic models according to their expressed equations. The plot of *ln* (q_e-q_t) versus *time* for pseudo-first-order kinetics exhibited linear regression: ln (q_e-q_t) = -0.0264t (min) - 2.2239, R^2 = 0.8655. where R^2 is the correlation coefficient [Figure 4a]. The plot of t/q_t versus *time* for pseudo-second-order kinetics demonstrated a linear regression equation: t/q_t (min g mg^{-1}) = 0.5043t (min) + 0.2151, R^2 = 1 [Figure 4b]. The plot of q_t versus *ln t* for Elovich kinetics illustrated a linear regression equation: q_t (mg g^{-1}) = 0.0384lnt + 1.8072, R^2 = 0.8409 [Figure 4c]. The plot of q_t versus $t^{0.5}$ for intra-particle diffusion kinetics provided a linear regression equation: q_t (mg g^{-1}) = 0.0129$t^{0.5}$ ($min^{0.5}$) + 1.8565, R^2 = 0.7527 [Figure 4d]. The variable parameters were determined by the respective equation and summarized in Table S1. The experimental data were best fitted with the pseudo-second-order kinetic model considering R^2 values, which confirmed that the adsorption process was carried out by a chemical reaction between CIP and ZGO (Ciopec *et al*., 2012; Li *et al*., 2017).

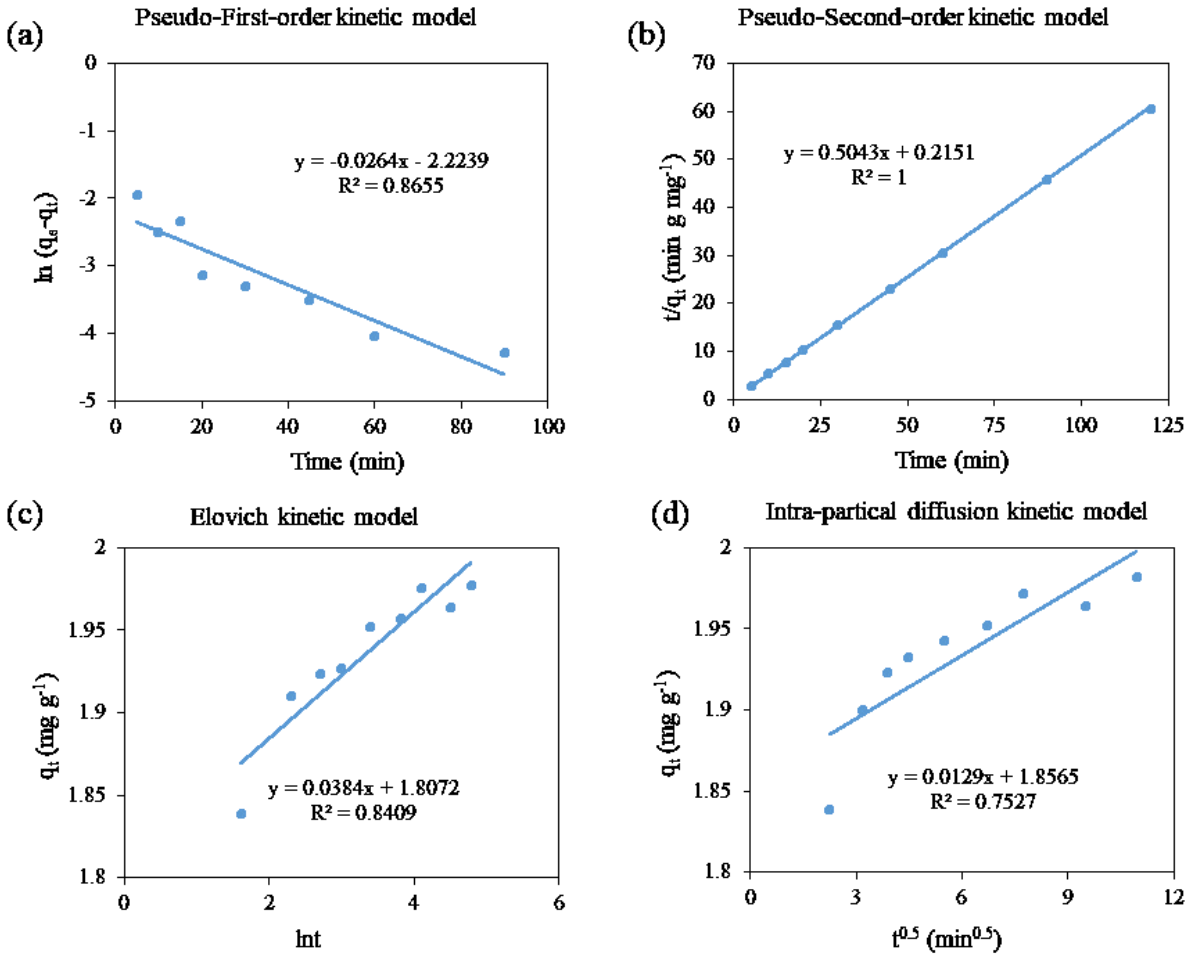

Figure 4: (a) Pseudo-first-order kinetic model, (b) pseudo-second-order kinetic model, (c) Elovich kinetic model, and (d) Weber−Morris intraparticle diffusion model [conditions: Co = 500 mg L^{-1}, pH = 7, ZGO = 0.25 g L^{-1}, t = (5−120) mins, shaking = 200 rpm, T = 32 °C].

3.2.5 *Adsorption Isotherms*

To study the adsorption behavior of CIP on ZGO and determine the capacity of the ZGO, the Langmuir, Freundlich, and Temkin isotherm models were considered and analyzed by different concentrations of CIP from 0.05 to 0.5 mg L^{-1} at constant temperature and constant pH (7.0). The simple form of the Langmuir isotherm (equation 8; where q_m is the maximum adsorption capacity of ZGO, mg g^{-1}; and K_L is the Langmuir adsorption constant, L mg^{-1}), the Freundlich isotherm (equation 9; where, K_F is the Freundlich adsorption constant, $mg^{1-1/n}$

$L^{-1/n}$ g^{-1}; and n is a constant related to adsorption intensity), and the Temkin isotherm (equation 10; where, R is the real gas constant, J K^{-1} mol^{-1}; T is the temperature, K; K_T refers the equilibrium binding constant, L g^{-1}; and b is the heat of adsorption constant, J mol^{-1}) are expressed as following equations (Kwak *et al*., 2016).

$$\frac{C_e}{q_e} = \frac{C_e}{q_m} + \frac{1}{K_L q_m} \quad (8)$$

$$\ln q_e = \ln K_F + \frac{1}{n} ln\, C_e \quad (9)$$

$$q_e = \frac{RT}{b} \ln K_T + \frac{RT}{b} \ln C_e \quad (10)$$

Figure 5 showed the calibration curves for 0.25 g L^{-1} adsorbent dose of ZGO while shaking at 20, 30, and 40 °C for three isotherm models according to their expressed equations. The plot of C_e/q_e versus C_e for the Langmuir isotherm demonstrated three linear regression equations with correlation coefficients of 0.9599, 0.9627, and 0.8837 for 20, 30, and 40 °C, respectively [Figure 5a]. The plot of $ln\ q_e$ versus $ln\ C_e$ for the Freundlich isotherm provided three linear regression equations with correlation coefficients of 0.9993, 0.9996, and 1.0000 for 20, 30, and 40 °C, respectively [Figure 5b]. The plot of q_e versus $ln\ C_e$ for the Temkin isotherm illustrated three linear regression equations with correlation coefficients of 0.8984, 0.9018, and 0.9137 for 20, 30, and 40 °C, respectively [Figure 5c]. The variable parameters were determined by the respective equation and summarized in Table S2. From the R^2 values of all isotherm models, experimental data best fitted to the Freundlich isotherm, which indicated that the adsorption of CIP happened on the multilayer and heterogeneous surface of ZGO (Yadav *et al*., 2018).

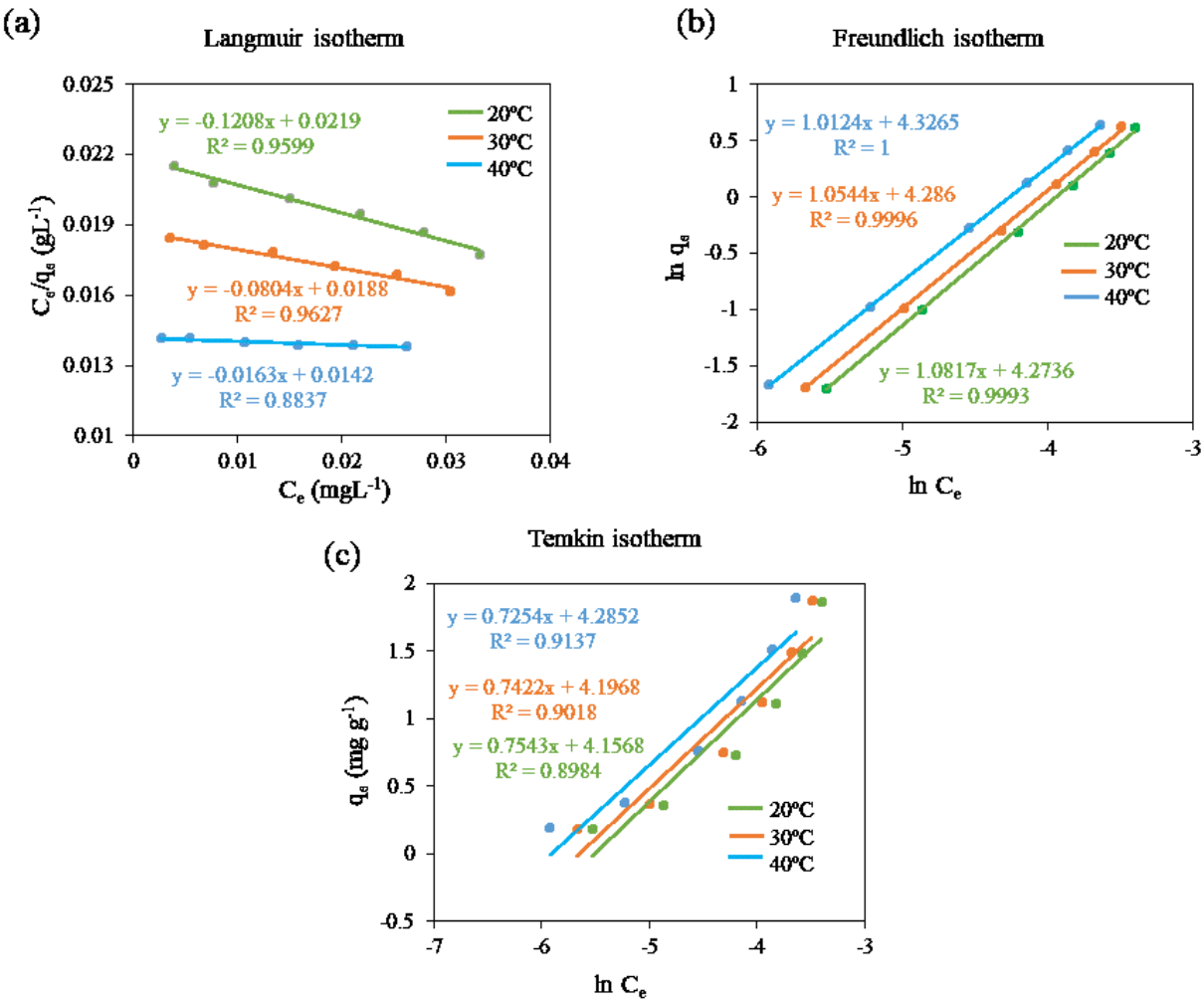

Figure 5: (a) Langmuir isotherms, (b) Freundlich isotherms, and (c) Temkin isotherm model (conditions: Co = 50−500 mg L^{-1}, pH = 7, ZGO = 0.25 g L^{-1}, t = 15 min, shaking = 200 rpm, T = 20, 30, and 40 °C).

The q_m was determined as 8.28, 12.45, and 61.35 mg g^{-1} for 20, 30, and 40 °C, respectively (as shown in Table S2), which confirmed the stimulation of greater sites of ZGO surface with the increment of temperatures during the adsorption process (Tang *et al*., 2013). Table 1 represents the comparison in the different parameters of ZGO with other previously reported adsorbents for CIP removal.

Table 1: Comparison in the different parameters of ZGO with other previously reported adsorbents for CIP removal.

Adsorbent	Fitted model		Optimum pH	Adsorption capacity (mg g^{-1})	References
	Kinetics	Isotherms			
Graphene oxide	Pseudo-2nd order	Langmuir	7	18.6	Yadav *et al*., 2018)
Reduced graphene oxide/magnetite composites	Pseudo-2nd order	Langmuir and Temkin	6.5	18.2	(Tang *et al*., 2013)
Chitosan/kaolin/ Fe_3O_4 magnetic microspheres	Pseudo-2nd order	Langmuir	6	47.8	(Ma *et al*., 2014)
Carbon nanofibers	Pseudo-2nd order	Langmuir	6	10.3	(Li *et al*., 2016)
Titanate nanotubes	Pseudo-2nd order	Langmuir	4	18.9	(Xu *et al*., 2019)
Clinoptilolite	Pseudo-2nd order	Langmuir	6	5.4	(Ngeno *et al*., 2019)
Carbon nanosheets supported TiO_2	Pseudo-2nd order	Freundlich	7	40.5	(Li *et al*., 2019)
MgO nanoparticles	Pseudo-2nd order	Langmuir	6	3.46	(Khoshnamvand *et al*., 2017)
ZGO nanoparticles	Pseudo-2nd order	Freundlich	7	61.35	This study

3.2.6 *Stability and Reusability*

Effects of stability and reusability of ZGO were examined several times regenerated after adsorption of CIP, and the decline of the removal percentage of CIP was shown in Figure S1. ZGO adsorbent demonstrated excellent removal percentage of CIP (~90%) for eleven consecutive sequences after washing by acetone every time. After first three cycles, the removal percentage of CIP moderately reduced 97.67% to 96.88%, then almost constant from forth to seven cycles (96.24-95.11%), but significantly decreased last five cycles. Because of strong stability and superior reusability, ZGO adsorbent could be considered as a potential candidate for real-time applications.

4. CONCLUSIONS

GO-functionalized zeolites (ZGO) were synthesized through a simple hydrothermal process for the adsorption of CIP from the aqueous solution. FESEM images revealed the scatter cubic-shaped zeolite NPs on the GO surface. FTIR and RAMAN demonstrated the successful formation of ZGO nanocomposites. The covalent bond between Al and/or Si with the different functional groups of GO (such as -COOH, -OH, and -C-O-C-) provided excellent results in 97.67% removal of CIP within only 15 min. Adsorption kinetics between ZGO and CIP followed the pseudo-second-order model, whereas experimental data best fitted to the Freundlich adsorption isotherm with a maximum q_m of 61.35 mg g^{-1} at the highest temperature (40 °C) of this study. In addition, ZGO adsorbent could be considered as a potential candidate for real-time applications owing to its remarkable stability and reusability.

ACKNOWLEDGEMENT

This research was financially supported by University Grants Commission (UGC) of Bangladesh (R&D ref. no. 37.01.0000.073.05.030.23.2960, date 20.12. 2023).

REFERENCES

Ahmed, M. B., Zhou J. L., Ngo H. H., and Guo W., 2015. Adsorptive removal of antibiotics from water and wastewater: Progress and challenges, *Sci. Total Environ*., 532, 112–126.

Akpotu, S. O., Oseghe E. O., and Ayanda O. S., 2019. Photocatalysis and biodegradation of pharmaceuticals in wastewater: effect of abiotic and biotic factors, *Clean Techn Environ Policy*, 21, 1701.

Alameri, A. A., Alfilh R. H. C., Awad S. A., Zaman G. S., Al-Musawi T. J., Joybari M. M., Balarak D., and McKay G., 2022. Ciprofloxacin Adsorption Using Magnetic and ZnO Nanoparticles Supported Activated Carbon Derived from Azolla Filiculoides Biomass, *Biomass Conv. Bioref*.

Al-Musawi, T. J., Mahvi A. H., and Khatibi A. D., 2021. Effective adsorption of ciprofloxacin antibiotic using powdered activated carbon magnetized by iron (III) oxide magnetic nanoparticles, *J Porous Mater*, 28, 835–852.

Antonelli, R., Geoffroy Roger P. M., Gurgel Carlos da Silva M., Melissa Gurgel A. V., 2020. Adsorption of ciprofloxacin onto thermally modified bentonite clay: Experimental design, characterization, and adsorbent regeneration, *J. Environ. Chem. Eng*., 8 (6), 104553.

Azam, M.G., Kabir M.H., Shaikh M.A.A., & Yasmin S., 2022. A rapid and efficient adsorptive removal of lead from water using Graphene Oxide prepared from waste dry cell battery, *J. Water Proc. Eng*., 46, 102597.

Banu, R., Swamy B. E. K., and Deepa S., 2020. Poly (fast sulphone black F) modified pencil graphite electrode sensor for serotonin, *Sensors International*, 1, 100044.

Biancullo, F., Moreira N. F., Ribeiro A. R., Manaia C. M., Faria J. L., Nunes O. C., Castro-Silva S. M., and Silva A. M., 2019. Heterogeneous photocatalysis using UVA-LEDs for the removal of antibiotics and antibiotic-resistant bacteria from urban wastewater treatment plant effluents, *Chem Eng J*., 367, 304-313.

Bui, T. X., Pham V. H., Le S. T., and Choi H., 2013. Adsorption of pharmaceuticals onto trimethylsilylated mesoporous SBA-15, *J. Hazard. Mater*., 254, 345-353.

Chen, H., Gao B., and Li H., 2015. Removal of sulfamethoxazole and ciprofloxacin from aqueous solutions by graphene oxide, *J. Hazard. Mater*., 282, 201–207.

Cheng, Z-L., Li Y-X., and Liu Z., 2017. Novel adsorption materials based on graphene oxide/Beta zeolite composite materials and their adsorption performance for rhodamine B, *J. Alloys Compd*., 708, 255-263.

Choudhury, P., Chattopadhyay S., De G., and Basu B., 2021. Ni–rGO–zeolite nanocomposite: an efficient heterogeneous catalyst for one-pot synthesis of triazoles in water, *Mater. Adv.,* **2,** 3042-3050.

Ciopec, M., Davidescu C. M., Negrea A., and Popa A., 2012. Adsorption studies of Cr (III) Ions from aqueous solutions by DEHPA impregnated onto Amberlite XAD7 − factorial design analysis, *Chem. Eng. Res. Des.*, 90, 1660−1670.

Cox, C. E., Marbury T. C., Pittman W. G., Brown G. L., Auerbach S. M., Fox B. C., and Yang J. Y., 2002. A randomized, double-blind, multicenter comparison of gatifloxacin versus ciprofloxacin in the treatment of complicated urinary tract infection and pyelonephritis, *Clin Ther*., 24, 223–236.

Dao, T. H., Tran T. T., Nguyen V. R., Pham T. N. M., Vu C. M., and Pham T. D., 2018. Removal of antibiotic from aqueous solution using synthesized TiO_2 nanoparticles: Characteristics and mechanisms, *Environ. Earth Sci*., 77, 359.

Diwan, V., Tamhankar A. J., Khandal R. K., Sen S., Aggarwal M., Marothi Y., Iyer R. V., Sundblad-Tonderski K., and StalsbyLundborg C., 2010. Antibiotics and antibiotic-resistant bacteria in waters associated with a hospital in Ujjain, India, *BMC Public Health*, 10, 414–421.

Espinosa, K., Park J. A., Gerrity J. J., Buono S., Shearer A., Dick C., Mak M. L., Teramoto K., Klausner J. D., Pandori M., and Hess D., 2015. Fluoroquinolone resistance in Neisseria gonorrhoeae after cessation of ciprofloxacin usage in San Francisco: using molecular typing to investigate strain turnover, *Sex Transm Dis*., 42, 57–63.

Farghali, M. A., Abo-Aly M. M., and Salaheldin T. A., 2021. Modified mesoporous zeolite-A/reduced graphene oxide nanocomposite for dual removal of methylene blue and Pb^{2+} ions from wastewater, *Inorg. Chem. Commun*., 126, 108487.

Ghosh, S., Pourebrahimi S., Malloum A., Ajala O. J., and Wani M. Y., 2023. A review on ciprofloxacin removal from wastewater as a pharmaceutical contaminant: Covering adsorption to advanced oxidation processes to computational studies, *Mater. Today Commun*., 37, 107500.

Grimes, K. L., Dunphy L. J., Loudermilk E. M., Melara A. J., Kolling G. L., Papin J. A., and Colosi L. M., 2019. Evaluating the efficacy of an algae-based treatment to mitigate elicitation of antibiotic resistance, *Chemosphere*, 237, 124421.

Gurunathan, S., Park J., Choi Y., and Kim J. -H., 2016. Synthesis of Graphene Oxide-Silver Nanoparticle Nanocomposites: An Efficient Novel Antibacterial Agent, *Curr. Nanosci*., 12, 762-773.

Homem, V., and Santos L., 2011. Degradation and removal methods of antibiotics from aqueous matrices—A review, *J. Environ. Manag*., 92, 2304.

Huang, X., Hu N., Gao R., and Zhang Y., 2012. Reduced graphene oxide–polyaniline hybrid: Preparation, characterization and its applications for ammonia gas sensing, *J. Mater. Chem*., 22, 22488.

Igwegbe, C. A., Oba S. N., Aniagor C. O., Adeniyi A. G., and Ighalo J. O., 2021. Adsorption of Ciprofloxacin from Water: A Comprehensive Review, *J. Ind. Eng. Chem.,* 93, 57.

Jara-Cobos, L., Abad-Delgado D., Ponce-Montalvo J., Menendez M., Peñafiel M. E., 2023. Removal of ciprofloxacin from an aqueous medium by adsorption on natural and hydrolyzed bentonites, *Front. Environ. Sci*., 11, 1239754.

Karthikeyan, S., Gupta V. K., Boopathy R., Titus A., and Sekaran G. A., 2012. New approach for the degradation of high concentration of aromatic amine by heterocatalytic Fenton oxidation: Kinetic and spectroscopic studies, *J. Mol. Liq*., 173, 153–163.

Khoshnamvand, N., Ahmadi S., and Mostafapour F. K., 2017. Kinetic and isotherm studies on ciprofloxacin an adsorption using magnesium oxide nanoparticles, *J. Appl. Pharm. Sci*., 7, 79–83.

Kummerer, K., Al-Ahmad A., and Mersch-Sundermann V., 2000. Biodegradability of some antibiotics, elimination of the genotoxicity and affection of wastewater bacteria in a simple test, *Chemosphere*, 40, 701–710.

Kümmerer, K., 2009. Antibiotics in the aquatic environment – A review – Part I, *Chemosphere*, 75, 417-434.

Kwak, H. W., Shin M., Yun H., and Lee K. H., 2016. Preparation of Silk Sericin/Lignin Blend Beads for the Removal of Hexavalent Chromium Ions, *Int. J. Mol. Sci.*, 17, 1466.

Le, T. H., Ng C., Tran N. H., Chen H., and Gin K.Y.H., 2018. Removal of antibiotic residues, antibiotic resistant bacteria and antibiotic resistance genes in municipal wastewater by membrane bioreactor systems, *Water Res*., 145, 498–508.

Li, W., Chuah C. Y., Kwon S., and Bae T. -H., 2020. Nanosizing Zeolite 5A Fillers in Mixed-Matrix Carbon Molecular Sieve Membranes to Improve Gas Separation Performance, *Chem. Eng. J. Adv*., 2, 100016.

Li, L., Zheng X., Chi Y., Wang Y., and Xu S. P., 2019. Molecularly imprinted carbon nanosheets supported TiO_2: strong selectivity and synergic adsorption photo-catalysis for antibiotics removal, *J. Hazard. Mater*., 383, 121211.

Li, S., Zhang X., and Huang Y., 2017. Zeolitic imidazolate framework-8 derived nanoporous carbon as an effective and recyclable adsorbent for removal of ciprofloxacin antibiotics from water, *J. Hazard. Mater.*, 321, 711-719.

Li, X. N., Wang W. Q., Dou J., and Zhao H. M., 2016. Dynamic adsorption of ciprofloxacin on carbon nanofibers: quantitative measurement by in situ fluorescence, *J. Water Process Eng*., 9, 14–20.

Ma, W., Dai J. D., Dai X. H., and Yan Y. S., 2014. Preparation and characterization of chitosan/kaolin/Fe_3O_4 magnetic microspheres and their application for the removal of ciprofloxacin, *Adsorpt. Sci. Technol*., 32, 775–790.

Magesh, N., Renita A. A., Kumar P. S., and Abraham L. S., 2022. Adsorption of ciprofloxacin from aqueous solution using surface improved tamarind shell as an economical and effective adsorbent, *Int. J. Phytoremediation*, 24, 224.

Mohammed, A. A., Atiya M. A., and Hussein M. A., 2019. Studies on membrane stability and extraction of ciprofloxacin from aqueous solution using pickering emulsion liquid membrane stabilized by magnetic nano-Fe_2O_3, *Colloids Surf. A: Physicochem. Eng.*, 585, 124044.

Mohiuddin, A. K., and Jeon S., 2022. Nitrogen-doped graphene supported α-$Co(OH)_2$ for sensitive determination of adrenaline, *ECS Adv*., 1, 046501.

Mohiuddin, A. K., Ahmed M. S., Roy N., and Jeon S., 2021. Electrochemical determination of hydrazine in surface water on $Co(OH)_2$ nanoparticles immobilized on functionalized graphene interference, *Appl. Surf. Sci.*, 540, 148346.

Mohiuddin, A. K., Yeasmin S., and Jeon S., 2023. Co_xNi_{1-x} double hydroxide decorated graphene NPs for simultaneous determination of dopamine and uric acid, *Sens. Actuator A Phys*., 355, 114314.

Moreira, N. F., Sousa J. M., Macedo G., Ribeiro A. R., Barreiros L., Pedrosa M., Faria J. L., Pereira M. F. R., Castro-Silva S., and Segundo M. A., 2016. Photocatalytic ozonation of urban wastewater and surface water using immobilized TiO_2 with LEDs: Micropollutants, antibiotic resistance genes and estrogenic activity, *Water Res*., 94, 10-22.

Ngeno, E. C., Shikuku V. O., Orata F., Baraza L. D., and Kimosop S. J., 2019. Caffeine and ciprofloxacin adsorption from water onto clinoptilolite: linear isotherms, kinetics, thermodynamic and mechanistic studies, *S. Afr. J. Chem.*, 72, 136–142.

Pham, T. D., Vu T. N., Nguyen H. L., Le P. H. P., and Hoang T. S., 2020. Adsorptive removal of antibiotic ciprofloxacin from aqueous solution using protein-modified nanosilica, *Polymers*, 12, 57.

Polesel, F., Andersen H. R., Trapp S., and Plósz B. G., 2016. Removal of Antibiotics in Biological Wastewater Treatment Systems A Critical Assessment Using the Activated Sludge Modeling Framework for Xenobiotics (ASM-X), *Int. J. Environ. Sci*., 50, 10316-10334.

Radjenović, J., Petrović M., Ventura F., and Barceló D., 2008. Rejection of pharmaceuticals in nanofiltration and reverse osmosis membrane drinking water treatment, *Water Res*., 42, 3601–3610.

Samal, K., Mahapatra S., and Ali M. H, 2022. Pharmaceutical wastewater as Emerging Contaminants (EC): Treatment technologies, impact on environment and human health, *Energy Nexus*, 6, 100076.

Samarghandi, M., Al-Musawi T., Mohseni-Bandpi A., and Zarrabi M., 2015. Adsorption of Cephalexin from Aqueous Solution Using Natural Zeolite and Zeolite Coated with Manganese Oxide Nanoparticles*, J. Mol. Liq*., 211, 431−441.

Sarangapani, C., Ziuzina D., Behan P., Boehm D., Gilmore B. F., Cullen P. J., and Bourke P., 2019. Degradation kinetics of cold plasma-treated antibiotics and their antimicrobial activity, *Sci. Rep*., 9, 1-15.

Tan, L., Wang S., Du W., and Hu T., 2016. Effect of water chemistries on adsorption of Cs (I) onto graphene oxide investigated by batch and modeling techniques, *Chem. Eng. J*., 292, 92-97.

Tang, K. L., Caffrey N. P., Nóbrega D. B., Cork S. C., Ronksley P. E., Barkema H. W., Polachek A. J., H. Ganshorn, Sharma N., Kellner J. D., and Ghali W. A., 2017. Restricting the use of antibiotics in food-producing animals and its associations with antibiotic resistance in food-producing animals and human beings: a systematic review and meta-analysis, *Lancet Planet Health 1*, e316-e327.

Tang, Y. L., Guo H. G., Xiao L., and Wang Y. L., 2013. Synthesis of reduced graphene oxide/magnetite composites and investigation of their adsorption performance of fluoroquinolone antibiotics, *Colloids Surf*., A 424, 74–80.

Tang, Y. L., Guo H. G., Xiao L., and Wang Y. L., 2013. Synthesis of reduced graphene oxide/magnetite composites and investigation of their adsorption performance of fluoroquinolone antibiotics, *Colloids Surf. A*, 424, 74–80.

Tran, Q. T., Do T. H., Ha X. L., Nguyen H. P. and Chau H. D., 2022. Study of the Ciprofloxacin Adsorption of Activated Carbon Prepared from Mangosteen Peel, *Appl. Sci*., 12, 8770.

Tran, N. H., Chen H., Reinhard M., Mao F., and Gin K. Y. H., 2016. Occurrence and removal of multiple classes of antibiotics and antimicrobial agents in biological wastewater treatment processes, *Water Res*., 104, 461– 472.

Tran, N. H., and Gin K. Y. H., 2017. Occurrence and removal of pharmaceuticals, hormones, personal care products, and endocrine disrupters in a full-scale water reclamation plant, *Sci. Total Environ*., 599, 1503.

Tran, N. H., Hoang L., Nghiem L. D., and Gin K. Y. H., 2019. Occurrence and risk assessment of multiple classes of antibiotics in urban canals and lakes in Hanoi, Vietnam, *Sci. Total Environ*., 692, 157–174.

Upoma, B. P., Yasmin S., Shaikh Md. A, A., and Kabir M. H., 2022. A Fast Adsorption of Azithromycin on Waste-Product-Derived Graphene Oxide Induced by H-Bonding and Electrostatic Interactions, *ACS Omega*, 7, 29655-29665.

Van Wieren, E.M., Seymour M.D., & Peterson J.W., 2012. Interaction of fluoroquinolone antibiotic, ofloxacin, with titanium oxide nanoparticles in water: Adsorption and breakdown, *Sci. Total Environ*., 441, 1-9.

Wahab, M., Zahoor M., Salman S. M., & Zekker I., 2021. Adsorption-membrane hybrid approach for the removal of Azithromycin from water: An attempt to minimize drug resistance problem, *Water*, 13, 1969.

Walker, D., Baumgartner D., Gerba C., and Fitzsimmons K., 2019. Surface Water Pollution. Environmental and Pollution Science (Third Edition*)*, 261-292.

Wang, F., Yang B., Wang H., Song Q., Tan F., and Cao Y., 2016. Removal of ciprofloxacin from aqueous solution by a magnetic chitosan grafted graphene oxide composite, *J. Mol. Liq*., 222, 188–194.

Yadav, S., Goel N., Kumar V., K. Tikoo, and Singhal S., 2018. Removal of fluoroquinolone from aqueous solution using graphene oxide: experimental and computational elucidation, *Environ. Sci. Pollut. Res*., 25, 2942–2957.

Yadav, S., Goel N., Kumar V., and K. Tikoo, Singhal S., 2018. Removal of fluoroquinolone from aqueous solution using graphene oxide: experimental and computational elucidation, *Environ. Sci. Pollut. Res*., 25, 2942–2957.Xu, X. M., Liu Y. X., Wang T., and Liu W., 2019. Co-adsorption of ciprofloxacin and Cu (II) onto titanate nanotubes: speciation variation and metal-organic complexation, *J. Mol. Liq*., 292, 111375.

Yu, Y., Murthy B. N., Shapter J. G., Constantopoulos K. T., Voelcker N. H., and Ellis A. V., 2013. Benzene carboxylic acid derivatized graphene oxide nanosheets on natural zeolites as effective adsorbents for cationic dye removal, *J. Hazard. Mater*., 260, 330-338.

Yu, Y., Murthy B. N., Shapter J. G., and Ellis A. V., 2013. Benzene carboxylic acid derivatized graphene oxide nanosheets on natural zeolites as effective adsorbents for cationic dye removal, *J. Hazard. Mater*., 260, 330-8.

Zhu, X., Tsang D. C. W., Chen F., Li S., and Yang X., 2015. Ciprofloxacin adsorption on graphene and granular activated carbon: kinetics, isotherms, and effects of solution chemistry, *Environ. Technol*., 36, 3094–3102.